Comparison Between Computer Simulation of Transport and Diffusion of Cloud Seeding Material Within Stratiform Cloud and the NOAA-14 Satellite Cloud Track

YU Xing[*1] (余 兴), DAI Jin[1] (戴 进), LEI Hengchi[2] (雷恒池), and FAN Peng[3] (樊 鹏)

[1]*Meteorological Institute of Shaanxi Province, Xi'an* 710015

[2]*Institute of Atmospheric Physics, Chinese Academy of Sciences, Beijing* 100029

[3]*Center for Weather Modification of Shaanxi Province, Xi'an* 710015

ABSTRACT

A precipitation enhancement operation using an aircraft was conducted from 1415 to 1549 LST 14 March 2000 in Shaanxi Province. The NOAA-14 satellite data received at 1535 LST soon after the cloud seeding shows that a vivid cloud track appears on the satellite image. The length, average width and maximum width of the cloud track are 301 km, 8.3 and 11 km, respectively. Using a three-dimensional numerical model of transport and diffusion of seeding material within stratiform clouds, the spatial concentration distribution characteristics of seeding material at different times, especially at the satellite receiving time, are simulated. The model results at the satellite receiving time are compared with the features of the cloud track. The transported position of the cloud seeding material coincides with the position of the track. The width, shape and extent of diffusion of the cloud seeding material are similar to that of the cloud track. The spatial variation of width is consistent with that of the track. The simulated length of each segment of the seeding line accords with the length of every segment of the track. Each segment of the cloud track corresponds to the transport and diffusion of each segment of the seeding line. These results suggest that the cloud track is the direct physical reflection of cloud seeding at the cloud top. The comparison demonstrates that the numerical model of transport and diffusion can simulate the main characteristics of transport and diffusion of seeding material, and the simulated results are sound and trustworthy. The area, volume, width, depth, and lateral diffusive rate corresponding to concentrations 1, 4, and 10 L^{-1} are simulated in order to understand the variations of influencing range.

Key words: NOAA satellite data, cloud track, transport and diffusion, numerical simulation, influencing range

1. Introduction

Transport and diffusion of seeding material in clouds is one of the main concerns of precipitation enhancement efforts. It is helpful in precipitation enhancement operations to understand the transport and diffusive characteristics of cloud seeding materials and to determine their transported positions and diffusive extent. Whether the seeding material can reach suitable positions and diffuse effectively is one of the major concerns of the operations (Levin et al., 1997; Li, 2002).

Bruintjes et al. (1999) pointed out that critical problems remain in the understanding of precipitation enhancement efforts and one of the fundamental problems is the diffusion and transport of seeding material throughout the cloud. First, the dispersion model for the boundary layer is used to simulate the transport and diffusion of seeding material in the cloud. This process is more complex than that of pollutants in the boundary layer so uncertainties still remain. Our understanding and knowledge about clouds is limited, including the transport and diffusion of material in the clouds. Second, real clouds cannot be formed in a cloud chamber to conduct fluid-dynamic experiments. The third is that gaseous tracer experiments are expensive and intricate and cannot yield representative integrated data. These make the numerical

E-mail: yuxing23@163.com

simulation lack an experimental foundation, and make the progress slow and cause some problems not to be solved appropriately.

The methodologies of transport and diffusion of seeding material in clouds generally include gaseous tracer experiments and numerical simulation. To determine the appropriate locations of the seeding lines with respect to the target areas, Gagin and Aroyo (1985) calculated the distance from the target area to the seeding line using a simple Gaussian plume dispersal method. From a series of wintertime airborne tracing experiments, Holroyd et al. (1988) determined some characteristics of the plumes of AgI smoke released either from the ground or from an aircraft over the Grand Mesa of Colorado. Bruintjes et al. (1995) calculated the targeting of tracer or seeding material over complex terrain in northern Arizona by a three-dimensional, time-dependent, nested-grid model. With trace chemical measurements of the silver content of snow, Warburton et al. (1995) investigated the transport and dispersion of AgI cloud seeding aerosols into and around two large target areas in the central Sierra Nevada. Shen and Chen (1987) simulated diffusion of catalytic agent released from an airplane by the Gaussian dispersion model under the assumption of homogeneous and steady flow fields and unlimited long line sources. Li and Pitter (1997) investigated the effects of different ice formation mechanisms on precipitation rate and patterns by plume dispersion based on diffusion rates specified by the Pasquill-Gifford neutral stability curves. Having estimated the fraction of seeding material that would manage to reach the proper levels in the clouds, Levin et al. (1997) used a mesoscale model to investigate the effectiveness of a broadcast static seeding method in Israel. For mimicking the seeding process, the airplane was depicted as a point source moving with a constant speed back and forth along the seeding line. Although the resolution of the model was good for mesoscale studies, it could not resolve individual plumes.

However, there are some important factors affecting transport and diffusion of seeding material in clouds including synoptic condition, airflow, wind shear, thermodynamics and dynamics. Generally, the diffusive rate of the seeding line is about $1\,\mathrm{m\,s^{-1}}$. The lateral spreading rates of aircraft-released AgI were estimated at over $2\,\mathrm{m\,s^{-1}}$ for cloudy conditions and less in clear conditions (Holroyd et al., 1988). Taking the heterogeneity and unsteadiness of meteorological fields, effects of topography, vertical wind shear, and temporal and spatial variation of seeding parameters into consideration, Yu et al. (1998, 2000) formulated a three-dimensional numerical model of transport and diffusion of seeding material within strati-

form clouds by combining a three-dimensional fine-grid non-hydrostatic mesoscale model. Although case simulation and sensitivity experiments were conducted, and the relationship between concentration distribution and mass conservation was discussed, no measurement or indirect proof demonstrated the validity and reliability of the model.

On 14 March 2000, a seeding operation for precipitation enhancement was carried out in Shaanxi Province. Fortunately, the NOAA-14 polar orbiting satellite gathered information on cloud tops after the cloud seeding. A cloud track appears on the satellite image. Its shape is very similar to the seeding line. To take advantage of this satellite data, the features of the NOAA National satellite image are analyzed first; secondly the simulated results of the transport and diffusion of the seeding material are compared with the satellite image features, and finally the simulation ability of the model is verified, and its validity is analyzed.

2. Model description

The model (Yu et al., 1998, 2000) consists of a puff trajectory model and a three-dimensional non-hydrostatic mesoscale model.

2.1 *The puff trajectory*

The puff trajectory model can deal with the temporal-spatial variation of source parameters with meteorological elements, and can be used to simulate the diffusion of all kinds of scales and sources (Ludwig et al., 1977; Ludwig, 1982). It is a practical and effective method for presenting the diffusion of pollutant sources. It is therefore introduced to simulate diffusion of seeding material within stratiform cloud.

The puff trajectory model represents line sources with a series of discrete puffs moving along the seeding line. The puff is idealized as a large ellipsoid. In order to partly consider the effect of vertical shear on diffusion, in the vertical direction, each puff is divided equally into 7 smaller puffs (sub-puffs). The mass or concentration of the 7 sub-puffs can be obtained by ellipsoidal integration:

$$Q_1 = Q_7 = 0.020Q_\mathrm{T}, \;\; Q_2 = Q_6 = 0.136Q_\mathrm{T},$$
$$Q_3 = Q_5 = 0.220Q_\mathrm{T}, \;\; Q_4 = 0.248Q_\mathrm{T}, \qquad (1)$$

where Q_T is the mass or amount of AgI particles of a puff. The diffusive parameters of each sub-puff depend on atmospheric turbulent diffusion on its grid; its movement observes a Lagrangian trajectory.

At any given time $t, u(t, x', y', z'), v(t, x', y', z'), w(t, x', y', z')$ are wind speed components at the sub-

puff center $[x'(t), y'(t), z'(t)]$; after time δt, the position of each sub-puff will be

$$x_s(t + \delta t) = x'(t) + u(t, x', y', z')\delta t , \qquad (2)$$

$$y_s(t + \delta t) = y'(t) + v(t, x', y', z')\delta t , \qquad (3)$$

$$z_s(t + \delta t) = z'(t) + w(t, x', y', z')\delta t , \qquad (4)$$

where δt is the calculation step, and the horizontal and vertical diffusive parameters σ_y, σ_z can be given by

$$\sigma_y^2(t + \delta t) = \sigma_y^2(t) + 2K_y(t, x_s, y_s, z_s)\delta t , \qquad (5)$$

$$\sigma_z^2(t + \delta t) = \sigma_z^2(t) + 2K_z(t, x_s, y_s, z_s)\delta t , \qquad (6)$$

where K_y, K_z are the diffusive coefficients in the horizontal and vertical directions.

The concentration of any sub-puff at any time t can be written as

$$C(t, x, y, z)_{nm} = \frac{Q_n}{(2\pi)^{3/2}\sigma_y^2\sigma_z}$$
$$\times \exp\left[-\frac{(x - x_s)^2 + (y - y_s)^2}{2\sigma_y^2} - \frac{(z - z_s)^2}{2\sigma_z^2}\right] , \quad (7)$$

where $n(= 1, 2 \ldots, 7)$ is the nth sub-puff; m is the mth puff, a function of time-wise segments; x, y, z are grid coordinates; Q_n is the amount of AgI particles of the nth sub-puff.

After the position of every sub-puff is determined in the simulated domain, temporal concentrations at a grid point can be calculated by superposing the sub-puff concentrations.

2.2 The mesoscale model

The accuracy and efficiency of the puff trajectory model depend on the accuracy of flow and turbulence fields, which are supplied by the non-hydrostatic mesoscale model. In order to accurately consider topographical effects, a terrain-following vertical coordinate system is used:

$$z_* = h_d(z - z_g)/(h_d - z_g) . \qquad (8)$$

where z_* and z are the transformed and Cartesian vertical coordinates, respectively; h_d is the height of model top; z_g is ground elevation.

The non-hydrostatic governing equations of the mesoscale model are composed of prognostic equations for velocity components, potential temperature and vapor, turbulent kinetic energy, dissipation rate and the anelastic continuity equation, following the coordinate transformation (Pielke and Martin, 1981). The diffusive coefficients are obtained by turbulent kinetic energy (E) and dissipation rate (ε) prognostic equa-

tions (Huang and Raman, 1989).

3. Simulation and result comparison

3.1 Cloud seeding and NOAA satellite data

On 14 March 2000, influenced by a frontal system, the middle part of Shaanxi Province was dominated by altostratus and altocumulus; there was sparse rain on the surface. From 1415 to 1549 LST, a seeding operation of precipitation enhancement was carried out in this area and its western neighbor by the Center for Weather Modification of Shaanxi Province. The operational aircraft was an An-26 with an airborne silver iodide acetone solution burner. The formula of operational seeding material is 20 g AgI, 6.2 g NH$_4$I, 879 g (1111 mL) acetone, 50 g water, 3.0 g NH$_4$ClO$_4$, 41.7 g NaClO$_4$, forming a ~2% concentration acetone solution of AgI.

The seeding started from A (Xi'an, 1415 LST) and passed B (Xianyang, 1419 LST), C (Wugong, 1433 LST), D (Linyou, 1442 LST), E (Fengxiang, 1448 LST), F (Longxian, 1459 LST), G (Baoji, 1508 LST), H (Liuba, 1521 LST), I (Lüeyang, 1535 LST), and J (Han zhong, 1549 LST) continuously (see Fig. 1). The first and second terms in the parentheses are the location name of the turning position on the surface and the seeding time (refer to Table 1) of the seeding line. The average flight speed for cloud seeding was 360 km h^{-1}. The seeding consumed 1200 g of AgI within 94 minutes. The seeding height was 4.35 km with a temperature of –10.0°C. The height of the cloud base was 2.2 km, where the temperature was 2.0°C. The cloud top ranged from 4.5 km to 5.0 km, whose temperature varied between –13.0°C and –17°C.

Because there was no measurement by Globe Positioning System (GPS), the seeding route was determined by the operation-recorded time and position. If the record is correct, the error is within several kilometers. It is reliable and available for the total cloud seeding length of several hundred kilometers and 1 km grid resolution.

During the course of cloud seeding, fortunately, the NOAA-14 satellite flew over this area. At 1535 LST, the satellite data were received by the Agricultural Remote Sensing Information Center of Xianyang City. A clear cloud track appeared on the satellite image (Fig. 2). After the imagery was rectified, it was synthesized from visible, near infrared and infrared channels 1, 2, and 4 with blue, green and red colors, respectively (Fig. 2). Points A', B', C', D', E' and G' are used to mark the turning points of the cloud track. E" and F" are marked replacing the turning point F' due to its indistinguishability resulting from the broken part around it. The even and flat cloud top (except around
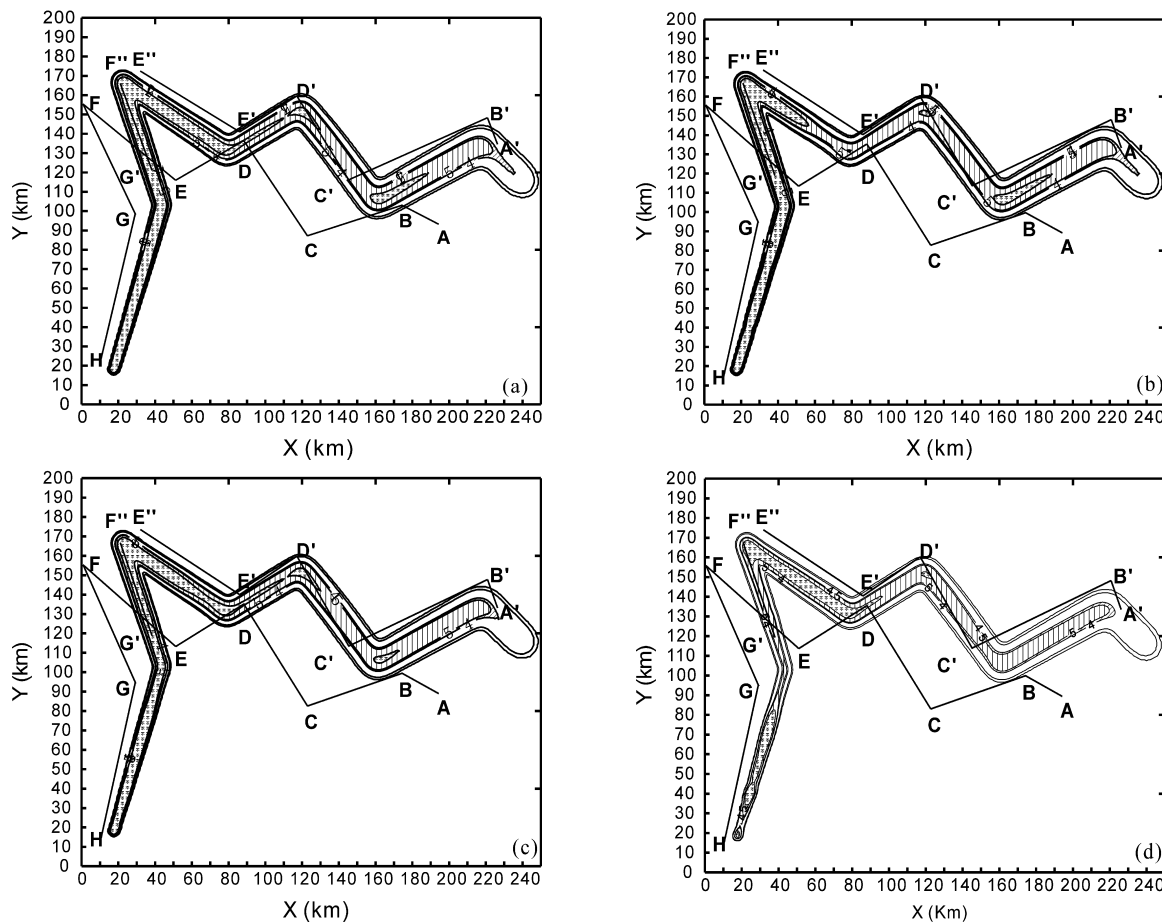
Fig. 1. Simulated concentration shape at 1535 LST: (a) projected onto the surface, (b) at the seeding altitude 4.35 km, (c) at 4.55 km, and (d) at 4.75 km. ABCDEFGH is seeding line, A'B'C'D'E'E"F"G' is the axial line of the cloud track. The concentration contours are 500, 100, 10, 5, 4, 1, 0.5 L^{-1}.

points E" and F") implied the cloud was stratiform. The turning points A', B', C', D', E', G' on the cloud track were distinguishable and clear. The cloud track was zigzag; the middle was wide and the two ends were narrow. The maximum width was 11 km (near C'), and the average width was 8.3 km. The widest part was located at C'D' and the latter portion of B'C', not A'B'. If the spatial variation of the cloud track was transformed into a temporal change, its width variations with time were rather narrower after the seeding material entered the cloud (around G'), then gradually became wide (E'E"), and becmae wider (C'D' and the latter portion of B'C'), diminished again (before B'C') until it disappeared (part of A'B'). These variations agree with the calculated effective range of cloud seeding (Yu et al., 2002).

Tracer experiments and airborne sampling only give information at different times and spatial points and cannot display the full profile on a cross section. However, the satellite image gives us a manifest and

complete panorama at the seeding cloud top at 1535 LST. With this satellite data, it is helpful and advantageous to verify the model of the transport and diffusion of seeding material, and especially the position of transported seeding material, the shape of the concentration distribution, and the diffusive extent of seeding material. The only limitation is that the magnitude of concentration at a given time and place cannot be confirmed.

3.2 Numerical simulation

Considering the receiving time of the NOAA data and the extent of the cloud track, the simulation horizontal domain is 33.50°–35.70°N，106.83°–109.50°E (250 km×250 km). AB, BC, CD, DE, EF, FG, and GH are chosen as 7 segments of the seeding line. The cloud seeding time until H was 66 minutes with 880 g AgI. The line source strength is 1.11×10^{13} s^{-1}, taking the nucleation activity as 5×10^{13} at a temperature of
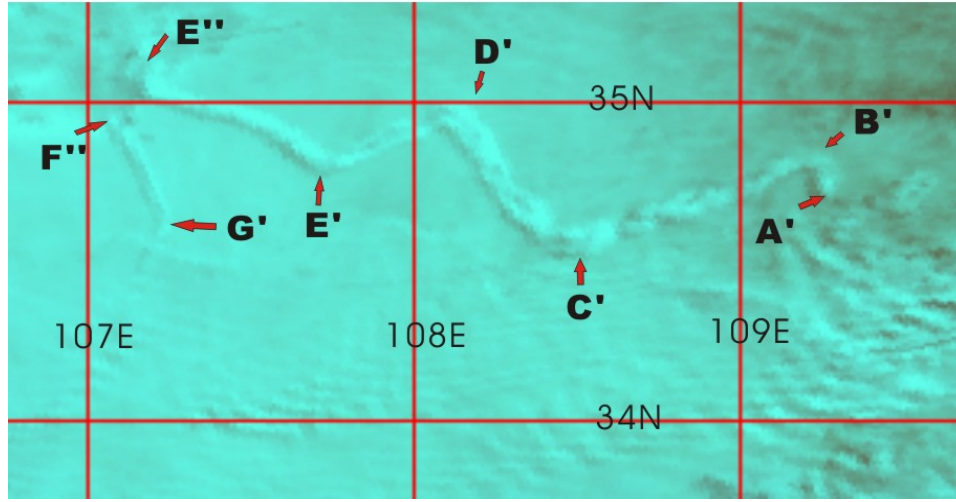
Fig. 2. Synthesized NOAA satellite imagery of seeded cloud.

–10°C. Because a fine grid is needed to distinguish the features of transport and diffusion of the seeding material, the horizontal and vertical grid intervals are 1 km, 0.2 km, and the time step is 20 s. The initial time and horizontal positions (X_{0m}, Y_{0m}) of the 7 segments of the seeding line entering the cloud are listed in Table 1. One puff is introduced into the model every 20 s, and the total number of puffs is 198. The particles of seeding material are assumed to be inert. Based on the meteorologically measured surface and sounding data at 0080 LST on that day, the predicted fields of wind and turbulence are input into the puff trajectory model to calculate the concentration distribution and variation of seeding material.

3.3 *Comparison between simulation result and cloud track*

The seeding material interacts with the droplets in the cloud, and causes the changes in the cloud. These changes are transmitted to the cloud top, and form the cloud track. The cloud track on the satellite image is a direct reflection of cloud top features. The seeding materials dispersing to different levels contribute to the cloud track, so a comparison between the features of the cloud track with the concentration on a given level will show a limitation. On the other hand, the position and width of the cloud track represent, to some extent, the transport and diffusion of seeding material, and there exists a response between them. It is reasonable to use the concentration projected onto the surface in the comparison.

Figure 1 displays the seeding material concentration projected onto the surface, at the seeding altitudes 4.35, 4.55, and 4.75 km at 1535 LST. At that time,

their transport positions and diffusive extent are consistent in the horizontal cross section, but their extents for a given concentration are different. The extent of a given concentration projected onto the surface is the maximum, and decreases next at 4.35 km, is third at 4.55 km, and is least at 4.75 km. The extent is rather wide at the seeding altitude and becomes narrower on the 4.55 and 4.75 km levels. The concentration distributions and magnitudes for each segment of the seeding line vary, and the distribution extent and position of a given concentration projected onto the surface is equivalent to that at the seeding altitude.

Comparing the simulated seeding line at 1535 LST with the cloud track, the extent and position coincide better with that of the cloud track, but the turning points shift southwards (Fig. 1a). The main reason may be that the wind direction at 0800 LST was westward at 500 hPa, the modeling u component is good and the v is smaller in the mesoscale model. The concentration axial lines of the cloud seeding lines BC, DE and EF are parallel to those of the cloud tracks B'C', D'E' and E'E", respectively, and the distances between axial lines BC and B'C', DE and D'E', EF and E'E" are 13.0, 6.5 and 11.4 km. The concentration axial line of CD crosses that of C'D', and FG almost coincides with F"G'. The transported positions of seeding material agree with the positions of the cloud track, and each segment of the seeding line corresponds with each segment of the cloud track, which suggests that the cloud track is caused by cloud seeding. The model can properly simulate the transport of the seeding line, and the mesoscale model can reasonably simulate the dynamical fields. In the cloud, the simulated average velocity components $u, v,$ and w are 9.96, 3.76, 3.7×

Table 1. The initial time (LST) and positions (X_{0m}, Y_{0m}) of 7 segments of the seeding line.

Positions	A	B	C	D	E	F	G	H
Time	1415	1419	1433	1442	1448	1459	1508	1521
X_{0m} (km)	192.9	173.4	122.2	86.8	50.4	0.0	27.5	9.3
Y_{0m} (km)	89.0	100.1	83.4	135.7	113.4	155.7	94.5	14.5

10^{-2} m s^{-1} and 9.64, 4.26, 4.1×10^{-2} m s^{-1} at 1400 and 1600 LST, respectively. There exists a weak updraft, which is intensified after the cloud seeding.

The widths and shapes of concentrations 4 and 5 L^{-1} are similar to those of the cloud track, and those of the concentration 4 L^{-1} are more similar. The shapes and the widths of concentrations greater than 10 L^{-1} or less than 1 L^{-1} are greatly different from those of the cloud track. All these imply that only when the concentration reaches a certain magnitude can the visible effect of seeding be obtained. With different clouds the concentration magnitude may be different. For this operational cloud seeding case, when the concentration is greater than or equal to 4 L^{-1}, the effect of cloud seeding will be obvious; if it is less than 1 L^{-1}, the effect of cloud seeding will be fainter. The simulated maximum widths corresponding to concentrations 1, 4, 5 L^{-1}, are 18.3 km (near the point B), 11.4 km (near the point C), and 10.6 km (near the point C), and their average widths are 12.9, 8.6, and 7.9 km, respectively. From this point of view, the shape of the concentration 4 L^{-1} is closer to that of the cloud track.

The concentration 4 L^{-1} (see the shading in Fig. 1) is wide at the middle and narrow at the ends. It agrees well with the width variation of the cloud track; the concentration widths of the seeding lines AB，FG, GH are rather narrow, and the ones of BC, CD, DE are rather wide. Correspondingly, the fore parts of A'B' and B'C' and the whole of F"G' of the cloud track are narrow, and the rear parts of B'C' and whole of C'D' and E'E" are wide.

The simulated seeding material concentrations projected onto the surface at different times are shown in Fig. 3. For concentration 4 L^{-1}, at 1445 LST, the seeding line DE is just entering the cloud; the extent is narrower, but the seeding line AB has been transported and diffused, its extent becomes gradually wider. At 1545 LST, part of line AB has disappeared and line CD has diminished from the maximum. The width variations with time of the concentration of seeding material match those of the cloud track (see section 3.1). These simulated width variations and those of the cloud track all suggest that the time for each segment of the seeding line diffusing to the maximum width is about 50 to 70 minutes.

Table 2 shows the length of the actual seeding line, seeding time, the length of the cloud track and the modeling line length of concentration 4 L^{-1}. The actual line length is distance calculated by latitude and longitude coordinates between two points, and the seeding time is the flight time between two points. The modeling lengths of seeding line AB, CD, DE, EF and FG are close to the length of the actual line, but BC and GH are longer by 11 km (20.4%) and 9 km (11.0%) than the actual seeding lines. The total modeling line length is 13 km (3.3%) longer than the total actual line length. However, the modeling lengths of line CD, DE and EF approach the length of the cloud track, while the modeling line length of BC is shorter by 18 km (21.7%), and those of AB and FG are longer by 7 km (46.7%) and 15 km (30%), than the corresponding segment lengths of the cloud track. The total modeling line length (excluding the segment of GH) is shorter by 18 km (6.0%) than the total lengths of the cloud track. The lengths CD, DE and EF of the cloud track are close to the length of the actual line with a shortage of 18 km (10.5%), while AB, BC and FG differ greatly from the actual seeding line.

A broken part on the cloud image around turning point F" causes the F' position to be incorrectly determined, and leads to a great length difference of 17 km (25.4%) between cloud track F"G' and the actual seeding line FG. However, the modeling FG length is only shorter by 2 km (3%) than its actual length.

At 1535 LST, after the seeding line AB transports and diffuses, the area of 4 L^{-1} gradually disappears, its width becomes narrow, and the modeling length is 22.0 km. The length of 5 L^{-1} is 5.4 km. The length of the cloud track A'B' is 15 km, shorter by 8 km (34.8%) than its actual length, and its shortening percentage is greater than that of C'D', D'E', E'F'. One of the reasons may be that the physical effect acting on the cloud top caused by the AB seeding line is decreasing. If that is true, it is reasonable that the period of influence of the AB seeding line is about 80 minutes; the area of influence disappears gradually after 80 minutes. The same reasoning can be used to judge the starting time of the cloud seeding action. On the satellite image (Fig. 2), the G' point can be distinguished although it is blurry, and the following cloud track, although fainter, can be identified by image magnification. The

point H' cannot be seen. The times of seeding points
G and H entering the cloud are 1508 and 1521 LST.
These results suggest that the seeding effect reaches
the cloud top after 15 to 25 minutes. Theoretically, it
is logical due to the fact that the activation of silver
iodide and the resulting physical effect take time.

The length of the cloud track and the modeling
length corresponding to the seeding line BC are longer
by 29 km (53.7%) and 11 km (20.4%) compared to its
actual length. Because there was no coordinate mea-
surement available, the seeding parameter was based
on the operational records. The recorded time of the

BC line was 14 minutes, the flight speed was
400 km h^{-1}, but the actual length was only 54 km, so
there is a great difference and an uncertainty about
them. Due to lack of any factor enlarging the seeding
line, the actual length of the seeding line may reach
80 km. The operational records show that the aircraft
flew from A passed the east of B, but there is no deter-
mined position for point B. The simulation describes
the seeding route according to the record. The record
indetermination of point B may lead to the error in
the simulated length, and this is why the concentra-
tion axial line of CD crosses with that of C'D'.
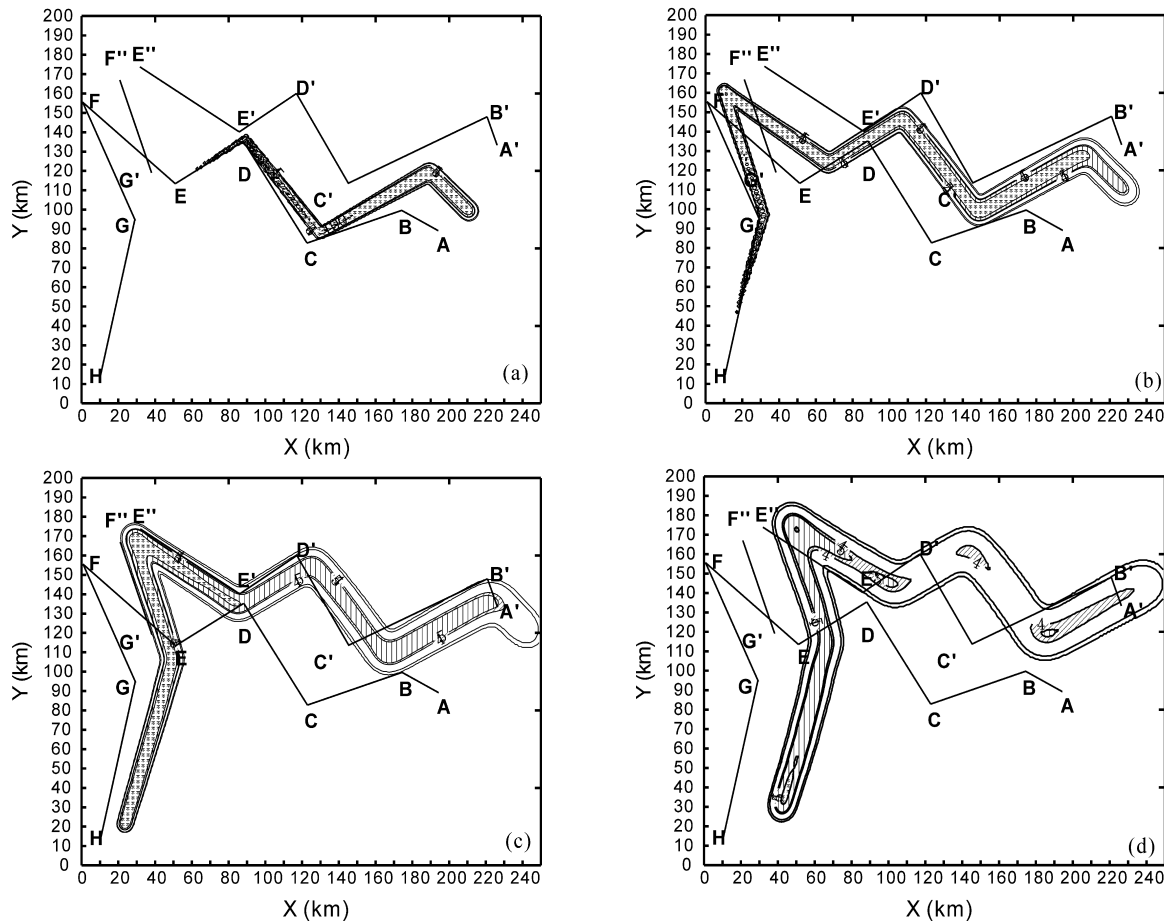
Fig. 3. Simulated concentrations projected onto the surface at (a) 1445, (b) 1515, (c) 1545, (d) 1615 LST; the others are as in Fig. 1.

Table 2. Length of the actual seeding line, of the cloud track and the modeling line.

Seeding line	AB	BC	CD	DE	EF	FG	GH	total
Actual line length (km)	23	54	63	43	66	67	82	398
Seeding time (min)	4	14	9	6	11	9	13	66
NOAA line length (km)	15	83	56	37	61	50	–	302
Modeling line length (km)	22	65	60	44	64	65	91	411

In summary, the transported position of the cloud seeding material coincides with the position of the cloud track. The width, shape and extent of diffusion of the cloud seeding material are similar to these of the track. The spatial variation of width is consistent with that of the cloud track. The simulated line length of each segment of the seeding line is in accordance with the length of each segment of the cloud track. Each segment of the cloud track corresponds with the transport and diffusion of each segment of the seeding line. These suggest that the cloud track is the direct physical reflection of cloud seeding at the cloud top. The comparison demonstrates that the numerical model of transport and diffusion can simulate the main characteristics of transport and diffusion of seeding material, and the simulated results are reasonable and trustworthy. If all segments of the seeding line are equally affected, the functioning time of the seeding material on every segment of the seeding line is about 80 minutes, which is significant in estimating the time of the effect of cloud seeding materials, especially in the design of the physical evaluation scheme. Beyond this time scope, even if the sampling measurement in the seeding area, the obvious physical effect may not be detected.

3.4 Influencing range of cloud seeding

The spatial and temporal distributions of width, extent, line length and position vary for different segments of the seeding line. For different concentrations at different levels or projected onto the surface, their influencing ranges including area, volume, depth and width can be obtained with the numerical simulation. These estimates are promising to determine target area, control and buffer region and to physically evaluate the seeding effect in the operation of precipitation enhancement.

Table 3 lists the simulated area, volume, width and depth corresponding to concentrations 1, 4, and 10 L^{-1} projected on the surface. The subscript denotes the concentration value. T stands for the time interval starting from 1415 LST. The average width and depth are divisions of area by the line length and of volume by area, respectively. At the same time, the high concentration covers a small area, volume, depth and width, while for low concentration, the influencing range is larger. For concentration $1\,L^{-1}$, the maximum width and the lateral diffusive rate for seeded segments of the seeding line is 21 km (at about 100 minutes) and 1.75 m s^{-1}. The maximum widths for seeded segments of the seeding line vary between 11.4 and 12.2 km (at about 65 minutes) for concentration $4\,L^{-1}$, and from 6.5 to 7.3 km (at about 40 min) for concentration $10\,L^{-1}$; consequently, their lateral diffusive rates vary from 1.46 to 1.56 m s^{-1}, and from 1.35 to 1.52 m s^{-1}, respectively.

4. Conclusions

For precipitation enhancement operation by an aircraft, the spatial concentration distribution characteristics of seeding material at different times are compared with the features of the cloud track. The following are the main conclusions.

Table 3. Simulated area $(S,\ \mathrm{km^2})$, volume $(V,\ \mathrm{km^3})$ width $(W,\ \mathrm{km})$ and depth $(D,\ \mathrm{km})$ for concentrations 1, 4, and 10 $\mathrm{L^{-1}}$.

T (min)	S_{10}	V_{10}	W_{10}	D_{10}	S_4	V_4	W_4	D_4	S_1	V_1	W_1	D_1
10	185	53.6	2.63	0.29	206	72.4	2.93	0.35	229	101.4	3.26	0.44
20	408	189.6	3.29	0.46	470	284.2	3.79	0.60	574	409.8	4.63	0.71
30	791	404.8	4.10	0.51	974	644.2	5.05	0.66	1171	983.2	6.08	0.84
40	1164	658.8	4.49	0.57	1521	1122.4	5.81	0.74	1905	1825.8	7.22	0.96
50	1472	877.0	4.98	0.60	2109	1690.8	6.64	0.80	2767	2998.6	8.62	1.08
60	1804	1034.2	5.05	0.57	2759	2332.2	7.16	0.85	3742	4419.0	9.61	1.18
70	1918	1006.8	4.92	0.52	3285	2882.8	7.84	0.88	4706	6033.0	11.06	1.28
80	1448	797.2	4.56	0.55	3534	3262.0	8.56	0.92	5486	7704.6	12.91	1.40
90	1124	629.2	5.01	0.56	3639	3413.4	9.19	0.94	6072	9217.4	14.43	1.52
100	754	379.4	4.35	0.50	3550	3238.4	9.06	0.91	6488	10530.0	15.78	1.62
110	371	170.2	4.24	0.46	3169	2724.0	8.64	0.86	6812	11706.6	16.89	1.72
120	65	16.2	2.60	0.25	2420	2009.6	7.77	0.83	7047	12570.0	17.77	1.78
Average	958.7	518.1	4.18	0.49	2303.0	1973.0	6.87	0.78	3916.6	5708.2	10.67	1.21

A vivid cloud track appears on the satellite image 80 minutes after the cloud seeding. Its length, average width and maximum width are 301 km, 8.3 and 11 km, respectively. This cloud track is a direct reflection of cloud seeding effect on the cloud top. It gives us a manifest and complete panorama of the seeded cloud top at that time.

The transported position of the cloud seeding material coincides with the position of the cloud track. The width, shape and extent of diffusion of the cloud seeding material are similar to that of the cloud track. The spatial variation of width is consistent with that of the track. The simulated line length of every segment of the seeding line is in accordance with the length of every segment of the cloud track. Every segment of the cloud track corresponds with the transport and diffusion of every segment of the seeding line. These suggest that the cloud track is indeed caused by the cloud seeding.

The comparison demonstrates that the numerical model of transport and diffusion can simulate the main characteristics of transport and diffusion of seeding material, and the simulated results are sound and trustworthy. The model can be applied to the simulation of transport and diffusion of seeding material within stratiform clouds.

The simulated area, volume, depth and width of influence are promising to determine the target area, control and buffer region and to physically evaluate the seeding effect in the operation of precipitation enhancement.

REFERENCES

Bruintjes, R. T., G. L. Kok, D. W. Breed, and V. Salazar, 1999: Hygroscopic seeding: Theory and practice. *Seventh WMO Scientific Conference on Weather Modification*, WMO/TD-No. 936, 65–68.

Bruintjes, R. T., T. L. Clark, and W. D. Hall, 1995: The dispersion of tracer plumes in mountainous regions in central Arizona: Comparisons between observations and modeling results. *J. Appl. Meteor.*, **34**, 971–988.

Gagin, A., and M. Aroyo, 1985: Quantitative diffusion estimates of cloud seeding nuclei released from airborne generators. *Journal of Weather Modification*, **17**, 59–70.

Holroyd, E. W., J. T. McPartland, and A. B. Super, 1988: Observations of silver iodide plumes over the Grand Mesa of Colorado. *J. Appl. Meteor.*, **27**, 1125–1144.

Huang, C. Y., and S. Raman, 1989: Application of the E-ε closure model to simulations of mesoscale topographic effects. *Bound.-Layer Meteor.*, **49**, 169–195.

Levin, Z., S. O. Krichak, and T. Reisin, 1997: Numerical simulation of disposal of inert seeding material in Israel using a three-dimensional mesoscale model. *J. Appl. Meteor.*, **36**, 474–484.

Li Dashan, 2002: *Status and Outlook of Weather Modification.* China Meteorological Press, Beijing, 586pp. (in Chinese)

Li, Z., and R. L. Pitter, 1997: Numerical comparison of two seeding material formation mechanisms on snowfall enhancement from ground-based aerosol generators. *J. Appl. Meteor.*, **36**, 70–85.

Ludwig, F. L., 1982: Effect of a change of atmospheric stability on the growth rate of puffs used in plume simulation models. *J. Appl. Meteor.*, **21**, 1371–1374.

Ludwig, F. L., L. S. Gasiorek, and R. E. Ruff, 1977: Simplification of a Gaussian puff model for real-time minicomputer use. *Atmos. Environ.*, **11**, 431–436.

Pielke, R. A., and C. L. Martin, 1981: The derivation of a terrain-following coordinate system for use in a hydrostatic model. *J. Atmos. Sci.*, **38**, 1707–1713.

Shen Yiming, and Chen Jihang, 1987: Numerical solution to the problem on diffusion of catalytic agent released from an airplane. *Acta Meteorologica Sinica*, **1**, 190–197.

Warburton, J. A, R. H. Stone, and B. L. Marler, 1995: How the transport and dispersion of AgI aerosols may affect detectability of seeding effects by statistical methods. *J. Appl. Meteor.*, **34**, 1929–1947.

Yu Xing, Fan Peng, Wang Xiaoling, Dai Jin, and Li Zhaoyuan, 1998: Numerical simulation of multiple line source diffusion of seeding agent within stratus. *Acta Meteorologica Sinica*, **56**, 190–197. (in Chinese)

Yu Xing, Dai Jin, Jiang Weimei, and Fan Peng, 2000: A three-dimensional model of transport and diffusion of seeding material within stratus. *Adv. Atmos. Sci.*, **17**, 617–635.

Yu Xing, Wang Xiaoling, and Dai Jin, 2002: Research on simulation of effective range for cloud seeding by aircraft within super-cool stratus. *Acta Meteorologica Sinica*, **60**, 205–214. (in Chinese)